Mineralogy and Petrology (2002) 74: 129–148

Mineralogy and Petrology

Stability range and decomposition of potassic richterite and phlogopite end members at 5–15 GPa

R. G. Trønnes

C. M. Scarfe Laboratory of Experimental Petrology, University of Alberta, Edmonton, Canada

With 7 Figures

Received April 10, 2000;
revised version accepted November 6, 2000

Summary

The phase relations of K-richterite, $KNaCaMg_5Si_8O_{22}(OH)_2$, and phlogopite, $K_3Mg_6Al_2Si_6O_{20}(OH)_2$, have been investigated at pressures of 5–15 GPa and temperatures of 1000–1500 °C. K-richterite is stable to about 1450 °C at 9–10 GPa, where the dp/dT-slope of the decomposition curve changes from positive to negative. At 1000 °C the alkali-rich, low-Al amphibole is stable to more than 14 GPa. Phlogopite has a more limited stability range with a maximum thermal stability limit of 1350 °C at 4–5 GPa and a pressure stability limit of 9–10 GPa at 1000 °C. The high-pressure decomposition reactions for both of the phases produce relatively small amounts of highly alkaline water-dominated fluids, in combination with mineral assemblages that are relatively close to the decomposing hydrous phase in bulk composition. In contrast, the incongruent melting of K-richterite and phlogopite in the 1–3 GPa range involves a larger proportion of hydrous silicate melts.

The K-richterite breakdown produces high-Ca pyroxene and orthoenstatite or clinoenstatite at all pressures above 4 GPa. At higher pressures additional phases are: wadeite-structured $K_2Si^{VI}Si^{IV}{}_3O_9$ at 10 GPa and 1500 °C, wadeite-structured $K_2Si^{VI}Si^{IV}{}_3O_9$ and phase X at 15 GPa and 1500 °C, and stishovite at 15 GPa and 1100 °C. The solid breakdown phases of phlogopite are dominated by pyrope and forsterite. At 9–10 GPa and 1100–1400 °C phase X is an additional phase, partly accompanied by clinoenstatite close to the decomposition curve. Phase X has variable composition. In the KCMSH-system ($K_2CaMg_5Si_8O_{22}(OH)_2$) investigated by *Inoue* et al. (1998) and in the KMASH-system investigated in this report the compositions are approximately $K_4Mg_8Si_8O_{25}(OH)_2$ and $K_{3.7}Mg_{7.4}Al_{0.6}Si_{8.0}O_{25}(OH)_2$, respectively.

Observations from natural compositions and from the phlogopite-diopside system indicate that phlogopite-clinopyroxene assemblages are stable along common

geothermal gradients (including subduction zones) to 8–9 GPa and are replaced by K-richterite at higher pressures. The stability relations of the pure end member phases of K-richterite and phlogopite are consistent with these observations, suggesting that K-richterite may be stable into the mantle transition zone, at least along colder slab geotherms. The breakdown of moderate proportions of K-richterite in peridotite in the upper part of the transition zone may be accompanied by the formation of the potassic and hydrous phase X. Additional hydrogen released by this breakdown may dissolve in wadsleyite. Therefore, very small amounts of hydrous fluids may be released during such a decomposition.

Introduction

Hydrous potassic phases such as phlogopite and potassic richterite are important carriers of hydrogen, halogens and alkalis in the upper mantle. The thermal stability fields of the phlogopite and K-richterite end members increase as a function of increasing pressure from 1 to 3 GPa, and reach temperatures of almost 1400 °C and more than 1200 °C, respectively at 2–3 GPa (*Yoder* and *Kushiro*, 1969; *Gilbert* and *Briggs*, 1974). At 5 GPa the stability limits of hydroxy- and fluorine end members of K-richterite reach 1275 °C and 1460 °C, respectively (*Foley*, 1991). *Huebner* and *Papike* (1970) synthesised KNa-richterites at a pressure of 0.1 GPa, and based on the measured molar volume of the products, they predicted that increasing pressure will tend to stabilise such amphiboles relative to phlogopite–pyroxene assemblages. Subsequent experimental studies demonstrated that the phlogopite–clinopyroxene assemblage is gradually replaced by potassic richterite and garnet at pressures above 8–9 GPa and temperatures of 1000–1300 °C (*Trønnes* et al., 1988; *Sudo* and *Tatsumi*, 1990; *Trønnes*, 1990; *Luth*, 1997; *Konzett* et al., 1997; *Konzett* and *Ulmer*, 1999). In subducting oceanic lithosphere, nearly all of the water and alkalis carried down to about 200 km depth by phlogopite is therefore likely to be carried further down to about 400 km depth by low-Al high-K amphibole.

In the Na-free system (*Sudo* and *Tatsumi*, 1990; *Luth*, 1997) the amphibole produced has a composition close to the KK-richterite component, $K_2CaMg_5Si_8O_{22}(OH)_2$. In Na-bearing natural compositions, however, the jadeite component of the pyroxene will contribute sodium to form the K-richterite component, $KNaCaMg_5Si_8O_{22}(OH)_2$, which predominates in low-Al amphiboles occurring in mantle xenoliths (*Erlank* et al., 1987; *Dawson*, 1987; *Harte*, 1987). In a simplified 7-component system (K_2O–Na_2O–CaO–MgO–Al_2O_3–SiO_2–H_2O, KNCMASH) representing the composition of phlogopite-bearing lherzolite the breakdown reaction can be written as:

$$\underset{\text{phlogopite}}{0.5\,K_2Mg_6Al_2Si_6O_{20}(OH)_4} + \underset{\substack{\text{in high-Ca px}\\ \text{(omphacite)}}}{CaMgSi_2O_6 + NaAlSi_2O_6} + \underset{\substack{\text{in low- or}\\ \text{high-Ca px}}}{2\,Mg_2Si_2O_6}$$
$$= \underset{\text{K-richterite}}{KnaCaMg_5Si_8O_{22}(OH)_2} + \underset{\text{in garnet}}{Mg_3Al_2Si_3O_{12}} \quad (1)$$

For this multivariant reaction, *Luth* et al. (1993) estimated a molar volume change of about −1.1 J/bar and a dp/dT-slope of approximately −20 bar/K. Such a slope is in general agreement with the breakdown curve (or breakdown zone) for the phlogopite-diopside assemblage determined by *Sudo* and *Tatsumi* (1990) and *Luth* (1997). In accordance with reaction (1), *Kushiro* and *Erlank* (1970) demonstrated experimentally that K-richterite is not stable in garnet-bearing assemblages at 2 GPa. The general lack of K-richterite in garnet-bearing mantle xenoliths (*Erlank* et al., 1987) indicates that the great majority of such xenoliths equilibrated at depths shallower than about 250 km before their ascent to the surface.

In order to assess further the relative stability ranges of phlogopite and K-richterite at pressures exceeding 5 GPa, it is instructive to consider the phase relations of the pure end member compositions as a function of pressure and temperature. *Sato* et al. (1997) and *Inoue* et al. (1998) investigated the stability and phase relations of a natural phlogopite containing 1.8% FeO and 1.3% F and the KK-richterite end member, respectively. This paper presents an experimental study of phase relations of phlogopite in the system KMASH and K-richterite in the system KNCMSH, described preliminarily by *Trønnes* et al. (1988) and *Trønnes* (1990). A reconnaicance study of the replacement of phlogopite + pyroxene by K-richterite + garnet in a phlogopite-doped peridotite composition described in *Trønnes* et al. (1988) and *Trønnes* (1990) will not be further discussed in this paper.

Experimental and analytical procedures

Starting materials

In order to investigate the possible effect of different starting materials on the stability of K-richterite and phlogopite, three types of material were used. Table 1 gives an overview of the experiments with type of starting material, pressure-temperature condition, pressure cell type, run duration, capsule material and resulting phase assemblage. Synthesized K-richterite, $KNaCaMg_5Si_8O_{22}(OH)_2$, and phlogopite, $K_2Mg_6Al_2Si_6O_{20}(OH)_4$, were used in most of the experiments. Some experiments were carried out with the same compositions as oxide mixes with H_2O and a corresponding amount of MgO present as brucite. A natural K-richterite (FRB836, provided by *F.R. Boyd*, Carnegie Inst.) was used in two of the experiments. The synthetic K-richterite and phlogopite were prepared as initial mixtures of SiO_2, Al_2O_3, MgO, $CaCO_3$, Na_2CO_3 and K_2CO_3. The oxide-carbonate mixes were ground in an agate mortar, decarbonatised and sintered before adding the appropriate amount of brucite. The synthesis of the K-richterite and phlogopite starting material was carried out in Pt-capsules in 19 mm diameter talc-pyrex furnace assemblies at 1.5 GPa and 1000 °C for 20–30 hr in an end-loaded piston cylinder apparatus. Powder X-ray diffraction analysis confirmed that the products were K-richterite and phlogopite without other detectable phases.

Experiments

The experiments were conducted using the uniaxial split-sphere apparatus (MA 6–8) at the University of Alberta, with a combination of 18/11, 14/8, 10/5 and

Table 1. *List of experiments*

Exp. #	p GPa	T °C	Conf type	Dur. min	Starting composition	Result (XRD)
68	4.5	1300	18-11	50	synth. Kr	Kr
333	4.5	1350	18-11	105	synth. Kr	Kr + di + en + fl
63	4.5	1400	18-11	30	synth. Kr	Kr + di + en + fl
					ox.mix Kr	Kr + di + en + fl
17	5.3	1000	18-11	20	synth. Kr	Kr
313	7.4	1400	18-11	45	synth. Kr	Kr
66	8.7	1200	14-8	50	ox.mix Kr	Kr synthesized
23	9.0	1000	18-11	58	synth. Kr	Kr
26	9.2	1200	18-11	120	synth. Kr	Kr
					natural Kr	Kr
27	9.2	1400	18-11	120	synth. Kr	Kr
					natural Kr	Kr
70	9.7	1500	14-8	34	synth. Kr	Kr + di + cen + wa + fl
28	9.8	1000	18-11	75	synth. Kr	Kr
					natural Kr	Kr
343	9.8	1360	18-11	50	synth. Kr	Kr
31	9.9	1000	18-11	140	synth. Kr	Kr
32	10.1	1000	18-11	100	synth. Kr	Kr
44	12.4	1200	14-8	90	ox.mix Kr	Kr synthesized
57	13.7	1200	14-8	20	synth. Kr	Kr
37	13.9	1000	14-8	28	synth. Kr	Kr
1343	14.5	1100	10-4	140	synth. Kr	Kr + di + cen + st + fl
159	15.0	1400	10-5	25	synth. Kr	di + cen + wa + X + fl
72	15.2	1100	14-8	20	synth. Kr	Kr + di + cen + st + fl
68	4.5	1300	18-11	50	ox.mix ph	ph synthesized
333	4.5	1350	18-11	105	synth. ph	ph
734	7.4	1000	18-11	135	synth. ph	ph
730	7.4	1200	18-11	90	synth. ph	ph
313	7.4	1400	18-11	45	synth. ph	ph + py + fo + fl
65	8.0	1200	14-8	50	ox.mix ph	ph synthesized
362	9.5	1100	18-11	24	synth. ph	ph + cen + py + fo + X + fl
70	9.7	1500	14-8	34	ox.mix ph	py + fo + fl
354	9.8	1250	18-11	70	synth. ph	py + X + fo + cen + fl
343	9.8	1360	18-11	50	synth. ph	py + X + fo + fl

WRe3–WRe25 thermocouples were used. Graphite capsules were used in experiments 57 and 66, whereas sealed platinum capsules were used in the other experiments. The thermocouple in exp. 159 failed and the experiment was held at a power consistent with the power–temperature relation for the 10–5 mm assembly. *Kr* K-richterite, *ph* phlogopite, *di* high-Ca pyroxene, *en* orthoenstatite, *cen* clinoenstatite, *st* stishovite, *py* prope, *fo* forsterite, *X* phase-X, *wa* wadeite-structured $K_2Si^{VI}Si^{IV}{}_3O_9$-phase, *fl* fluid

10/4 mm assemblies. Most of the experiments were conducted in double capsule assemblies, similar to those described by *Wei* et al. (1990), and several of these experiments had pressure calibrants in the second sample capsule. A more detailed account of the 18/11 mm pressure cell assembly and the thermal gradients across the sample capsules is found in *Wei* et al. (1990). Based on the recommended revision of the coesite-stishovite transition by *Zhang* et al. (1996), the pressure calibration used in this paper is adjusted relative to the calibration in the preliminary reports of *Trønnes* et al. (1988) and *Trønnes* (1990). The revised pressure calibration curves at 1000 °C for the 18 and 14 mm assemblies are based on the following phase transitions: fayalite (α–γ) at 5.3 GPa (*Yagi* et al., 1987), coesite–sishovite at 8.7 GPa (*Zhang* et al., 1996) and forsterite to wadsleyite at 13.8 GPa (*Akaogi* et al., 1989; *Katsura* and *Ito*, 1989; *Fei* et al., 1991). The pressure calibration curve for the 10/4 mm assembly is presented by *Trønnes* (2000). The precision of the sample pressures is estimated to be $\pm$0.5 GPa.

The temperature was measured by WRe_3–WRe_{25} thermocouples, inserted radially through the cylindrical heaters in the 18 and 14 mm assemblies (e.g. *Wei* et al., 1990) and axially in the 10 mm assemblies (*Trønnes*, 2000). No correction was made for the pressure effect on the thermocouple EMF. The temperature was stable within $\pm$10 °C during the 20–140 min long experiments. Two-pyroxene thermometry experiments indicate that the thermal gradients within the sample capsules are about 50 °C/mm. The rate of heating during the approach to run temperature was 60–80 °C/min.

In most of the experiments the samples were contained in sealed Pt capsules. Two experiments (run numbers 57 and 66) on the K-richterite composition, however, were conducted in unsealed graphite capsules. In order to minimise the potential diffusion of hydrogen from the sample material, the pressure cell parts were not fired prior to the experiments. The experimental products in the graphite capsules did not differ from those of the Pt capsules. K-richterite was synthesised in one of the graphite capsule experiment using the oxide mix with brucite as a starting material (Run 66, Table 1).

Sample characterisation

After the experiments the sample capsules were cut longitudinally for examination. All of the run products were investigated by powder X-ray diffraction, and several of them were embedded in epoxy, sectioned and polished for electron microscopy and major element microanalysis. The mineral chemical compositions reported in Tables 2 and 3 were analysed with a Jeol 733X Superprobe with 4 wavelength-dispersive spectrometers at the joint facility of IKU Petroleum Research and the Geological Survey of Norway in Trondheim. The instrument operated at an accelerating voltage of 15 kV with a beam current of 15 nA and counting time of 20 s on the peaks. The raw data were corrected by a ZAF program. Standards used were wollastonite for Ca and Si, kyanite for Al, olivine for Mg, albite for Na and orthoclase for K. The minerals were analysed with a raster mode of analysis covering areas of up to 10 μm^2. Based on repeated spot analyses of samples and standards (5–15 analyses of each phase), the estimated precision and accuracy (1σ) range from about 2% for elements present at abundance levels exceeding 10 wt% to 10–15% for elements present at abundance levels less than 1 wt%.

Table 2. *Composition of minerals in the K-richterite system*

Run #, conditions		SiO_2	MgO	CaO	Na_2O	K_2O	$\sum_{wt\%}$	Si	Mg	Ca	Na	K	$\sum_{cat}$
Theoretical bulk composition		57.6	24.2	6.72	3.71	5.64	97.87	8.00	5.00	1.00	1.00	1.00	16.00
68, 4.5 GPa–1300 °C	Kr	56.9	24.2	6.66	3.72	5.47	97.0	7.98	5.05	1.00	1.01	0.98	16.02
	di	57.3	23.7	18.6	0.44	0.04	100.1	2.02	1.25	0.70	0.03	–	4.00
	en	60.1	338.8	1.82	0.06	0.03	100.8	2.00	1.93	0.07	–	–	4.00
333, 4.5–1350	Kr	57.3	23.8	6.35	3.87	5.46	96.8	8.03	4.97	0.95	1.05	0.98	15.98
	di	56.9	23.4	18.7	0.67	0.18	99.9	2.01	1.24	0.71	0.05	0.01	4.01
	en	59.6	38.2	1.64	0.03	0.02	99.5	2.01	1.92	0.06	–	–	3.99
313, 7.6–1400	Kr	57.7	24.3	6.95	3.68	5.62	98.3	7.98	5.01	1.03	0.99	0.99	16.01
70, 10.0–1500	di	56.7	21.5	20.3	0.84	0.25	99.6	2.02	1.14	0.78	0.06	0.01	4.01
	cen	60.0	39.2	0.92	0.04	0.03	100.2	2.01	1.95	0.03	–	–	4.00
	wa	72.1	0.23	0.15	0.52	27.4	100.4	3.99	0.02	0.01	0.06	1.93	6.01
1343, 14.5–1100	Kr	58.0	23.9	6.57	3.84	5.85	98.2	8.03	4.93	0.98	1.03	1.03	16.00
	di	56.4	18.8	22.4	1.29	0.33	99.2	2.04	1.01	0.87	0.09	0.02	4.02
	cen	60.0	39.9	0.15	0.06	0.03	100.1	2.00	1.99	0.01	–	–	4.00

Oxides in weight%, cations normalized to a total charge of 46 (23 O-atoms) for K-richterite, 8 for pyroxene and 18 for wadeite-structured $K_2Si^{VI}Si^{IV}{}_3O_9$ phase. The phase compositions are average values of 5–10 analyses. Based on repeated spot analyses of samples and standards, the estimated precision and accuracy (1σ) range from about 2% for elements present at abundance levels exceeding 10 wt% to 10–15% for elements present at abundance levels less than 1 wt%. Abbreviations as in Table 1

Table 3. *Composition of minerals in the phlogopite system*

Run #, conditions		SiO_2	Al_2O_3	MgO	K_2O	$\sum_{wt\%}$	Si	Al	Mg	K	$\sum_{cat}$
Theoretical bulk composition		43.2	12.2	29.0	11.3	95.7	6.00	2.00	6.00	2.00	16.00
333, 4.5–1350	ph	42.8	13.3	28.0	10.9	95.0	5.97	2.19	5.82	1.94	15.91
734, 7.4–1000	ph	43.4	13.4	28.2	10.9	95.9	5.99	2.18	5.80	1.92	15.88
313, 7.4–1400	py	45.1	24.2	30.3	–	99.6	3.04	1.92	3.04	–	8.00
	fo	43.1	0.10	57.5	–	100.7	1.00	–	1.99	–	3.00
362, 9.5–1100	ph	43.2	12.3	28.2	11.1	94.8	6.04	2.03	5.88	1.98	15.93
	py	45.7	23.4	30.8	–	99.9	3.07	1.85	3.08	–	8.01
	cen	59.5	0.60	39.4	–	99.5	1.00	0.01	0.99	–	2.00
	X	47.8	2.83	29.8	17.6	98.1	7.95	0.56	7.4	3.73	19.64
343, 9.8–1360	py	45.8	23.2	30.8	–	99.8	3.08	1.84	3.09	–	8.00
	X	48.0	2.95	29.9	17.1	98.0	7.96	0.58	7.40	3.62	19.56
	fo	42.2	0.31	57.3	–	99.8	0.99	0.01	2.01	–	3.01
70, 9.7–1500	py	45.8	23.5	30.9	–	100.2	3.07	1.86	3.09	–	8.01

Oxides in weight%, cations normalized to a total charge of 44 (22 O-atoms) for phlogopite, 24 for pyrope, 8 for forsterite, 6 for clinoenstatite and 52 for phase X. The phase compositions are average values of 5–10 analyses. Based on repeated spot analyses of samples and standards, the estimated precision and accuracy (1σ) range from about 2% for elements present at abundance levels exceeding 10 wt% to 10–15% for for elements present at abundance levels less than 1 wt%. Abbreviations as in Table 1

Phase relations

General features

The experimental results are listed in Table 1 and the resulting phase diagrams for the K-richterite and phlogopite compositions are shown as Fig. 1 and Fig. 2, respectively. The dashed breakdown curves for K-richterite and phlogopite (Figs. 1, 2) represent the approximate locations for these curves. The breakdown curves will have inflections at the locations where changes occur in the breakdown mineral assemblage. These inflection points are not sufficiently constrained by the present data set.

The listed phase assemblages indicate that the breakdown reactions are mostly divariant for the 6-component K-richterite (KNCMSH) system and the 5-component phlogopite (KMASH) system, although the phlogopite decomposition above 8 GPa may be univariant. A divariant breakdown implies that the reaction will occur gradually over some distance in p-T space. Alternatively, if there are additional, small amounts of undetected phase(s) in the run products, the apparent decomposition reactions may still appear to be gradual because of the thermal

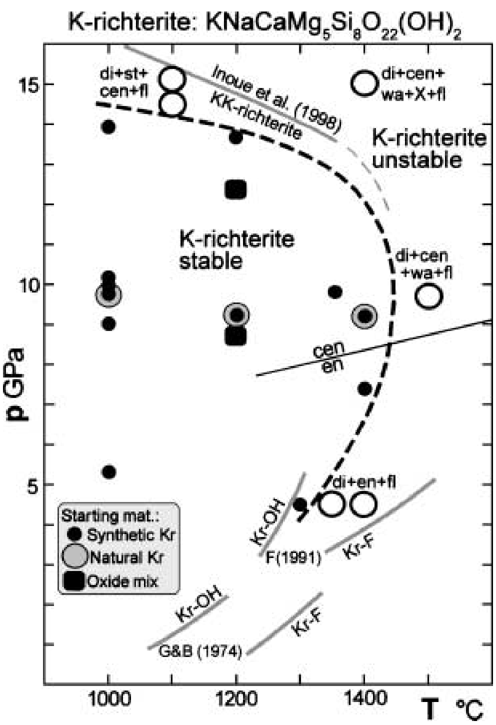

Fig. 1. Phase diagram of the system K-richterite $KNaCaMg_5Si_8O_{22}(OH)_2$. The orthoenstatite (en) – high-P clinoenstatite (cen) boundary is from *Pacalo* and *Gasparik* (1990) and *Shinmei* et al. (1999). Different symbols within the stability field of K-richterite indicate different starting materials. Abbreviations and other details are presented in Table 1. Breakdown curves in the 1–2 GPa and 3–5 GPa ranges are shown for comparison: G&B(1974): *Gilbert* and *Briggs* (1974); F(1991): *Foley* (1991); Kr–OH: hydroxyl K-richterite end member; Kr–F: fluorine K-richterite end member. The low-pressure incongruent melting of K-richterite at 1–2 GPa produces forsterite + diopside + melt

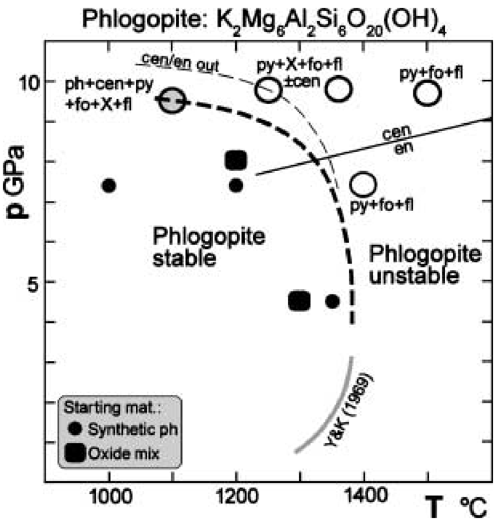

Fig. 2. Phase diagram of the system phlogopite $K_2Mg_6Al_2Si_6O_{20}(OH)_4$. The orthoenstatite (en) – high-p clinoenstatite (cen) boundary is from *Pacalo* and *Gasparik* (1990) and *Shinmei* et al. (1999). Different symbols within the stability field of phlogopite indicate different starting materials. Abbreviations and other details are presented in Table 1. The incongruent melting curve of phlogopite in the 1–3 GPa range, producing forsterite + melt, is shown for comparison: Y&K(1969): *Yoder* and *Kushiro* (1969)

gradients in the sample capsules. Both of these features may explain the fact that K-richterite and phlogopite is present in the cooler ends of many of the sample capsules run at p-T conditions to the right and above the decomposition curves. The result column in Table 1 lists the mineral assemblage (largely from powder X-ray diffraction), including K-richterite and phlogopite in these experiments. The only experiments where all of the K-richterite and phlogopite are decomposed are experiment number 159 (15.0 GPa, 1400 °C) for the K-richterite system and experiments 70, 354 and 343 (9.7–9.8 GPa, 1250–1500 °C) for the phlogopite system.

Small amounts of additional phases are observed in some of the products from experiments inside the shown stability ranges of K-richterite and phlogopite. These phases are undetectable by powder X-ray diffraction, even on low-background, single crystal quartz base plates. For experiments below, but close to the decomposition curve, such additional phases present at the hot end of the capsule (e.g. diopside and enstatite in experiment 68) signify the initial decomposition of K-richterite or phlogopite. The presence of small amounts of additional phases can also result from a deviation in the K-richterite and phlogopite compositions from the theoretical end member stoichiometry (see Tables 2 and 3).

In both systems the fluid phases that form during the high-pressure breakdown reactions quench to fine-grained aggregates of very alkali- and water-rich flaky mineral grains. These grains and mineral aggregates undergo rapid decomposition under an electron beam, and can therefore not be analysed reliably. The high-pressure fluid phases in these systems have considerably higher water and alkali contents than the liquid formed during melting in the phlogopite + diopside system (*Luth*, 1997 and discussion below). Therefore, such phases are referred to as fluid rather than melt in this paper.

K-richterite

Figure 1 illustrates the close correspondence between the inferred decomposition curve (decomposition zone) of K-richterite above 4.5 GPa and the decomposition curves for the 1–2 GPa and 3–5 GPa ranges determined by *Gilbert* and *Briggs* (1974) and *Foley* (1991). These two lower-pressure studies determined the breakdown relations for both OH- and F-components of the K-richterite. The thermal stability limit of the F-component is elevated by about 150 °C relative to the OH-component in the 1–5 GPa pressure range. The three experiments carried out on the natural K-richterite within the stability range of the synthetic end member all resulted in a single phase amphibole.

The high-pressure decomposition curve for the KK-richterite, $K_2CaMg_5Si_8O_{22}(OH)_2$, determined by *Inoue* et al. (1998) is also shown in the figure. It appears that the KK-component is stable to a pressure that is about 1 GPa higher than for the KNa-component in the 13–15 GPa range.

According to *Gilbert* and *Briggs* (1974) and *Foley* (1991), the low-pressure breakdown of K-richterite involves the formation of forsterite, diopside and liquid at 1–2 GPa and enstatite, diopside and liquid at 3.5–5 GPa. The 5 GPa decomposition assemblage of *Foley* (1991) is identical to the 4.5 GPa assemblage in this study. Figure 3 shows the breakdown products orthoenstatite and high-Ca amphibole (diopside) in the hot end of the sample capsule of experiment 333 (4.5 GPa). The fluid phase appears as a fine-grained aggregate of alkali-rich hydrous quench products between laths of orthoenstatite and high-Ca pyroxene. At pressures above 9 GPa, the breakdown assemblage includes high-Ca pyroxene, clinoenstatite, wadeite-structured $K_2Si^{VI}Si^{IV}{}_3O_9$ (see also *Inoue* et al., 1998), and fluid. At 15 GPa and 1400 °C phase X (*Kushiro* et al., 1967; *Trønnes*, 1990; *Luth*, 1997; *Konzett* and

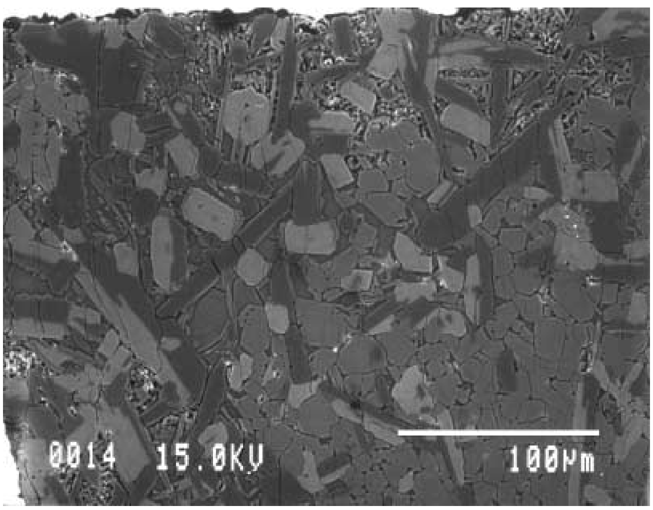

Fig. 3. Back-scattered electron (BSE) image of run products of experiment 333 (4.5 GPa, 1350 °C, K-richterite composition). The K-richterite (medium BSE-intensity, medium grey) is still present in the lower, cooler part of the capsule. Laths of enstatite (dark) and diopside (light) with interstitial quenched fluid (fine grained aggregate) occur along the hot wall of the capsule. Scale bar is 100 μm

Yang, 1998; *Inoue* et al., 1998; *Konzett* and *Fei*, 2000) occurs in addition to these minerals. The breakdown reaction at 1100 °C and 14–15 GPa produces high-Ca pyroxene, clinoenstatite, stishovite and fluid.

Phlogopite

The phase relations and inferred decomposition curve of phlogopite is shown in Fig. 2. The decomposition curve is nearly coincident with that of a natural phlogopite, $K_{2.1}Na_{0.1}Mg_{5.4}Fe_{0.2}Al_{2.5}Si_{5.7}O_{20}(OH,F)_4$, in the 4–8 GPa range (*Sato* et al., 1997). The curve for the breakdown of phlogopite to forsterite and melt in the 1–3 GPa range (*Yoder* and *Kushiro*, 1969) is shown for reference. The dominant high-pressure breakdown phases of phlogopite is pyrope and forsterite (Figs. 4, 5). Additional breakdown products in the form of clinoenstatite and phase X are present at 9–10 GPa (Fig. 6). Clinoenstatite reacts out relatively close to the breakdown curve and disappears completely at lower pressure. Enstatite was not observed as a breakdown product in the natural phlogopite system in the 4–8 GPa range by *Sato* et al. (1997).

Another small difference between the observations in the pure end member system of this study and the natural phlogopite composition is the phase relations at temperatures below the main decomposition curve. Whereas *Sato* et al. (1997) observed an incipient breakdown of the natural phlogopite to pyrope and fluid at pressures of 5–8 GPa and temperatures at 1200–1300 °C, the pure phlogopite end member appears to remain stable in this p-T interval. The amount of pyrope observed below the main phlogopite-out curve for the natural phlogopite composition, however, is very low, ranging from less than 5 vol% at 5 GPa to 30 vol% at 8 GPa. This increase in pyrope content with increasing pressure is reflected in a

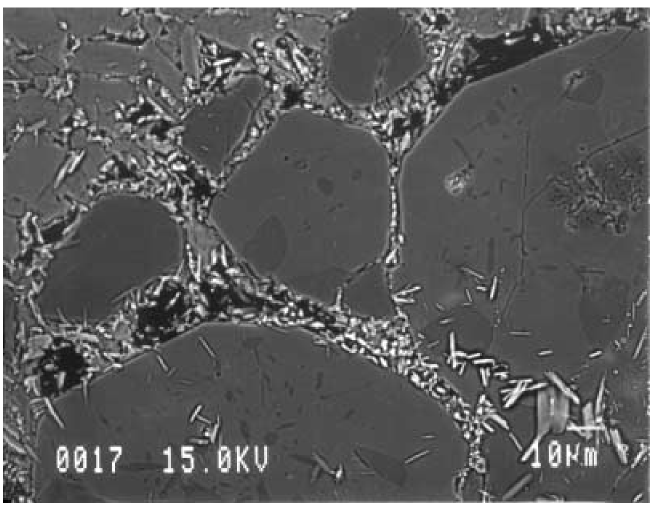

Fig. 4. BSE image of experiment 313 (7.4 GPa, 1400 °C, phlogopite composition), cooler part of capsule. Large, rounded grains of pyrope with irregular inclusions of forsterite (dark patches) with phlogopite (intermediate BSE intensity) in the upper left hand corner. The fine-grained aggregates of bright (from edge effects) alkali- and water-rich laths represent the quenched fluid. Scale bar is 10 μm

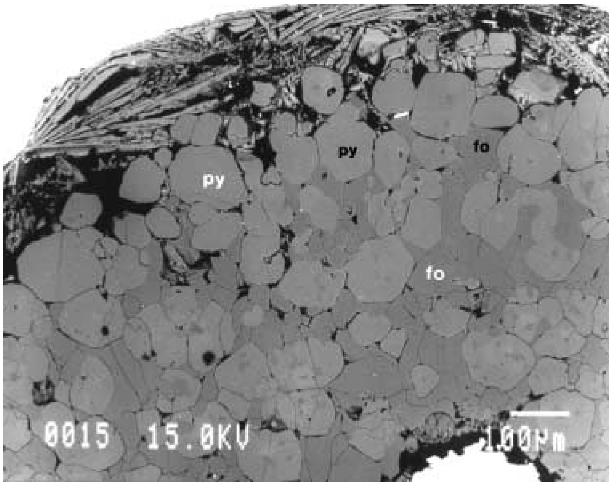

Fig. 5. BSE image of experiment 70 (9.7 GPa, 1500 °C, phlogopite composition), view covering most of the charge. Pyrope (py) and forsterite (fo), with quenched fluid products along the upper Pt wall. All of the phlogopite has disappeared. Scale bar is 100 μm

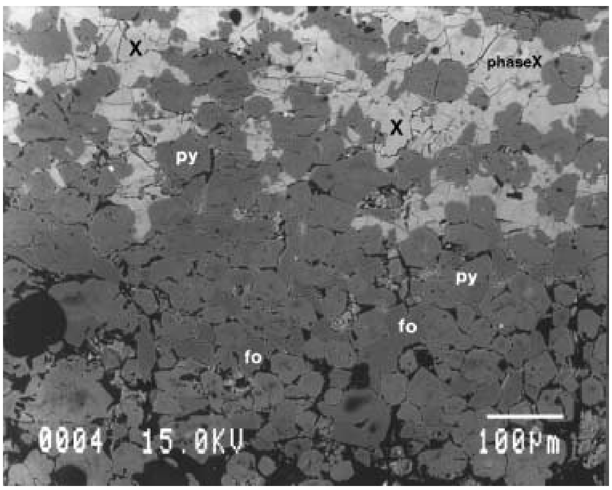

Fig. 6. BSE image of experiment 343 (9.8 GPa, 1360 °C, phlogopite composition). Phase X (high BSE intensity in the upper, cooler part of the capsule. Pyrope (py) and forsterite (fo) dominate the lower, hotter part. Scale bar is 100 μm

systematic change in the composition of the coexisting phlogopite (see the discussion below).

Mineral compositions

KNCMSH-system

A representative selection of mineral compositions for the K-richterite system (KNCMSH) is presented in Table 2. The K-richterite composition does not vary systematically as a function of pressure and temperature and is identical to that of the ideal end member within the analytical uncertainty. *Inoue* et al. (1998) observed a similar constant composition close to the ideal end member (bulk composition) in their study of the KK-richterite system.

The compositions of the coexisting pyroxenes also correspond to those of the KK-richterite system studied by *Inoue* et al. (1998). The mole fraction of diopside in the high-Ca pyroxenes ranges from 0.36 to 0.46, indicating that the coexisting pyroxenes are far from chemical equilibrium at these moderate temperatures of 1100–1500 °C (e.g. *Gasparik*, 1990).

The K_2O-contents of 0.04–0.33 wt% in the high-Ca pyroxenes are lower than those of the clinopyroxenes in the phlogopite-diopside system (0.2–0.9 wt%, *Luth*, 1997) and in the KK-richterite system (0.1–0.7 wt%, *Inoue* et al., 1998). In contrast to the Na-free KCMASH- and KCMSH-systems however, the KNCMSH-system has high-Ca pyroxenes with 0.4–1.3 wt% Na_2O. The Na- and K-contents of the high-Ca pyroxenes both increase with increasing pressure. The substitution mechanism(s) for Na and K in the Al-free KNCMAH-system are also different from the Al-bearing systems where the jadeite and "K-jadeite" components seem to dominate (*Harlow*, 1997; *Luth*, 1997).

Further electron microprobe analyses of the uncharacterised K–Si-phase occurring in the 9–15 GPa range and described by *Trønnes* (1990) demonstrate that this is close to $K_2Si_4O_9$. No crystal structural information is available for this minor phase. *Kinomura* et al. (1975) demonstrated that a $K_2Si^{VI}Si^{IV}{}_3O_9$-phase is isostructural with wadeite ($K_2Zr^{VI}Si^{IV}{}_3O_9$) at high P and T, and *Fasshauer* et al. (1998) contributed new thermodynamic data and revised the phase relations in the KAS-system. *Inoue* et al. (1998) observed a similar $K_2Si_4O_9$-phase in their experimental products in the KK-richterite system. Phase X, present only in experiment 159, was identified from a powder X-ray diffraction pattern similar to those of phase X in the run products from about 10 GPa in the phlogopite system. Mineral compositions of this run product are not available, but *Inoue* et al. (1998) reports a composition close to $K_4Mg_8Si_8O_{25}(OH)_2$ in the KK-richterite system. The phase X grains produced by *Konzett* and *Fei* (2000) have similar compositions but very variable $K/(K+Na)$ ratios.

KMASH-system

Table 3 lists representative mineral compositions for the phlogopite system. By analogy with the K-richterite system, the phlogopite compositions in the KMASH-system are very similar to the phlogopite end member composition (and starting composition). No obvious systematic compositional change as a function of pressure or temperature is observed, except for a weak suggestion of increased Si/Al ratio with increasing pressure. These observations are supported by the results from the phlogopite–diopside system (*Luth*, 1997), where the analysed phlogopite composition also is similar to the phlogopite end member.

Table 3 shows that the pyrope compositions are also very similar to the theoretical pyrope end member. Increasing pressure appears to cause a weak tendency towards slightly more majoritic garnet from about 4 mole% enstatite at 7.4 GPa to about 8 mole% at 9.8 GPa. These enstatite contents are consistent with the values derived from other experimental studies (*Fei* and *Bertka*, 1999).

Forsterite and clinoenstatite have compositions very similar to the theoretical end members, and do not exhibit any systematic variations. The composition of phase X is close to $K_{3.7}Mg_{7.4}Al_{0.6}Si_{8.0}O_{26}$, with very little variation between the two compositions representing a temperature variation of 260 °C at a nearly constant pressure (9.5–9.8 GPa). The experimental studies of *Konzett* and *Fei* (2000) and *Luth* (1997) demonstrate considerable variation in the composition of phase X. The variation is not strictly and simply connected to the variation in pressure and temperature, although the analyses presented by *Luth* (1997) indicate a variation from $K_{2.2}Mg_{6.7}Al_{1.8}Si_{7.7}O_{26}$ at 11 GPa to $K_{3.3}Mg_{7.0}Al_{0.3}Si_{8.4}O_{26}$ at 17 GPa. The oxide sums of his analyses are generally lower (average 94.2 wt%) than those of *Inoue* et al. (1998), *Konzett* and *Fei* (2000) and this study (Table 3, average 98.0 wt%). *Konzett* and *Yang* (1998) established a hexagonal unit cell for phase X and concluded that its composition can be quite variable.

Discussion

The decomposition reactions for K-richterite and phlogopite produces alkali- and water-dominated fluids in addition to the solid breakdown phases. This is indicated by the nature of the quench products in the form of fine-grained aggregates of flaky and unstable Na–K–H-dominated crystals (Figs. 3–5). Relatively low volumes of alkali- and water-rich fluid compositions are also indicated by the observed combination of solid breakdown phases and the inferred decomposition reactions. It is possible to put approximate *lower limits* on the amounts of oxides dissolved in the fluid phases. Ignoring the details of the mineral compositions involved, the following approximate end member reactions may apply:

$$\underset{\text{K-richterite}}{KNaCaMg_5Si_8O_{22}(OH)_2} = \underset{\text{diopside}}{CaMgSi_2O_6} + \underset{\text{enstatite}}{2Mg_2Si_2O_6} + \underset{\text{fluid}}{0.5K_2O + 0.5Na_2O + 2SiO_2 + H_2O} \quad (2)$$

$$\underset{\text{K-richterite}}{KNaCaMg_5Si_8O_{22}(OH)_2} = \underset{\text{diopside}}{CaMgSi_2O_6} + \underset{\text{enstatite}}{2Mg_2Si_2O_6} + \underset{\text{wadeite-structure}}{0.5K_2Si_4O_9} + \underset{\text{fluid}}{0.5Na_2O + H_2O} \quad (3)$$

$$\underset{\text{phlogopite}}{K_2Mg_6Al_2Si_6O_{20}(OH)_4} = \underset{\text{pyrope}}{Mg_3Al_2Si_3O_{12}} + \underset{\text{forsterite}}{Mg_2SiO_4} + \underset{\text{fluid}}{K_2O + MgO + 2SiO_2 + 2H_2O} \quad (4)$$

$$\underset{\text{phlogopite}}{K_2Mg_6Al_2Si_6O_{20}(OH)_4} = \underset{\text{pyrope}}{Mg_3Al_2Si_3O_{12}} + \underset{\text{forsterite}}{Mg_2SiO_4} + \underset{\text{enstatite}}{MgSiO_3} + \underset{\text{fluid}}{K_2O + SiO_2 + 2H_2O} \tag{5}$$

$$\underset{\text{phlogopite}}{K_2Mg_6Al_2Si_6O_{20}(OH)_4} = \underset{\text{pyrope}}{Mg_3Al_2Si_3O_{12}} + \tfrac{3}{8}\ \underset{\text{phaseX}}{K_4Mg_8Si_8O_{25}(OH)_2} + \underset{\text{fluid}}{\tfrac{1}{4}\ K_2O + \tfrac{13}{8}\ H_2O} \tag{6}$$

Equations (2) and (3) represent the K-richterite decomposition at about 5 and 10 GPa, respectively. The breakdown of phlogopite below 8 GPa is represented by equation (4). Equations (5) and (6) in various combinations illustrate the phlogopite decomposition above 8 GPa. The theoretical weight percentages of the fluid phase in the decomposition assemblages are 26, 6, 35, 23 and 6% in the reactions (2) to (6), respectively. Thus, the breakdown reactions occurring in the highest pressure regions may involve the smallest amounts of fluids and therefore also the fluids that are most enriched in alkalis and water. In practice, the fluid proportions will be larger than the minimum values representing these theoretical decomposition reactions, because significant amounts of additional oxides will be dissolved in the fluids.

In contrast to the high-pressure breakdown of K-richterite and phlogopite, the low-pressure decomposition reactions produce larger fractions of hydrous silicate melts. In the lower pressure range of 1–3 GPa K-richterite and phlogopite melt incongruently to forsterite + diopside + melt and forsterite + melt, respectively (*Gilbert* and *Briggs*, 1974; *Yoder* and *Kushiro*, 1969). The melting reactions K-richterite = 2 forsterite + diopside + fluid and phlogopite = 3 forsterite + fluid produce a minimum of 40 and 49 wt% hydrous melt, respectively.

It is important to note that the phlogopite and the K-richterite end members are similar to the mica and amphibole phases that are stable in these experiments, and that there are only minor variations in the composition of these phases as a function of pressure and temperature. An experimental investigation of a contact metamorphic, natural phlogopite composition $K_{2.06}Na_{0.09}Mg_{5.36}Fe_{0.22}Ti_{0.04}Al^{VI}{}_{0.26}Al^{IV}{}_{2.26}Si_{5.74}O_{20}(OH, F)_4$, with 1.28 wt% F by *Sato* et al. (1997) contrasts with the above observations. In that study the analysed phlogopites change systematically from a composition close to the starting material at 4 GPa to a composition more similar to the phlogopite end member at 8 GPa. This compositional trend involves decreasing Al in combination with increasing Si and Mg, and is consistent with the accompanying production of pyrope and fluid. The minor differences in the phase relations of the natural phlogopite studied by *Sato* et al. (1997) and the phlogopite end member of this study can therefore largely be explained by the deviation of the natural phlogopite composition from that of the phlogopite that is stable under high pressure conditions. *Sato* et al. (1997) suggest the following decomposition of the ideal phlogopite component to explain the formation of minor amounts of pyrope and fluid in the subsolidus region with increasing pressure from 5 to 8 GPa:

$$\underset{\text{phlogopite}}{K_2Mg_6Al_2Si_6O_{20}(OH)_4} = \underset{\text{pyrope}}{Mg_3Al_2Si_3O_{12}} + \tfrac{3}{7}\ \underset{\text{hypothetical phlogopite}}{K_2Mg_7Si_7O_{20}(OH)_4} + \underset{\text{fluid}}{\tfrac{4}{7}\ K_2O + \tfrac{8}{7}\ H_2O} \quad (7)$$

The equivalent equation presented by *Sato* et al. (1997) contains some printing errors. The corrected equation (7) illustrates the production of phlogopite with increasing concentrations of Si and Mg and decreasing Al-content from 4 to 8 GPa and 1250–1300 °C, in accordance with the observed trend. A more realistic equation with the same effects, however, would place the $K_2Mg_6Al_2Si_6O_{20}(OH)_4$-component on the right hand side of the equation and a starting composition with higher Al and lower Si and Mg on the left hand side.

Furthermore, the natural phlogopite composition investigated by *Sato* et al. (1997) seems to be characterised by more extensive production of fluid (or silicate melt) than the end member phlogopite system. This inference is based on the fact that their experiment at 8 GPa and 1350 °C did not contain enstatite and that the experiment at 6 GPa and 1500 °C contained only pyrope and fluid. The presence of elements such as iron and fluorine will probably promote more extensive melting or fluid production in this system after most of the phlogopite has reacted out. The thermal stability limits of this natural phlogopite and the phlogopite end member at 4–8 GPa, however, are very similar. This can be explained by the combination of the stabilising effect of F and the destabilising effect of Fe.

The extension of the stability range of K-richterite beyond the decomposition pressure of phlogopite has important implications for the recycling of alkalis and water in the Earth's upper mantle. Figure 7 summarises the stability fields of phlogopite, K-richterite and KK-richterite, along with the curves for the disappearance of these phases in the system diopside-phlogopite, which is more relevant to the Earth's upper mantle. Various geothermal gradients, in the form of cold and hot slabs (*Peacock*, 1991), Archean shield and average mantle adiabat (*McKenzie* and *Bickle*, 1988) are shown for reference. In a subduction zone environment, phlogopite will gradually disappear by reaction with pyroxene component(s) (diopside or dioside + jadeite + enstatite, see equation 1) at pressures ranging from 7 to 10 GPa. KK-richterite, however, remains stable in the presence of garnet to pressures of 12–14 GPa (*Luth*, 1997). The upper stability limit of the pure K-richterite component appears to be about 1 GPa lower than that of KK-richterite (*Inoue* et al., 1998; this work). Even so, K-richterite may persist in cold slab environments below the 410 km discontinuity where wadsleyite becomes a dominant phase. The ultimate breakdown of K-richterite in this region may produce small amounts of phase X. Due to the high solubility of H in wadsleyite-type structures (*Inoue* et al., 1995; *Smyth* and *Kawamoto*, 1997) the release of a water-rich fluid phase is not a necessary outcome of this decomposition. The amount of phase X that may be produced will depend on the amount of Na that can be incorporated and the composition of this phase can be quite variable with

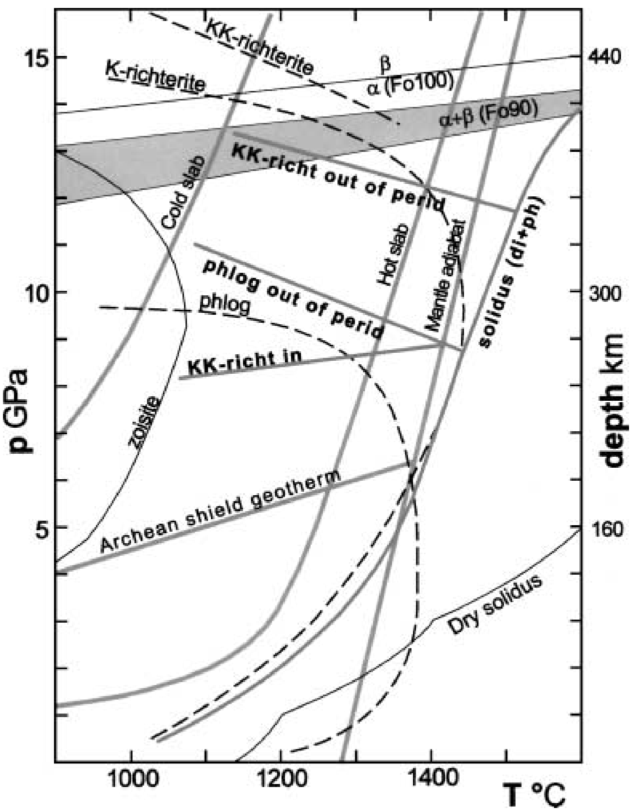

Fig. 7. Stability relations of phlogopite and K-richterite, as single phases and as part of mantle mineral assemblages. Stippled curves from Figs. 1 and 2 show the stability limits of phlogopite, K-richterite and KK-richterite (this study and *Inoue* et al., 1998). The thick dark lines and curve represent the model peridotite system diopside-phlogopite (*Sudo* and *Tatsumi*, 1991; *Luth*, 1997). Various lines representing the gradual reaction phlogopite + pyroxene = K-richterite + garnet are based on *Luth* (1997): KK-richterite in, Phlogopite out of peridotite, and KK-richterite out of peridotite. Four different geothermal gradients are shown as thick gray lines (*Luth* et al., 1993): cold slab and hot slab (*Peacock*, 1991), average mantle adiabat and Archean shield (*McKenzie* and *Bickle*, 1988). The olivine (α) to wadsleyite (β) transition in pure forsterite (Fo_{100}) and the $\alpha + \beta$ phase loop in the composition Fo_{90} is from *Fei* et al. (1991). The stability field of zoisite and the dry peridotite solidus are from *Pawley* (1994) and *Herzberg* et al. (1990), respectively

$K/(K + Na)$ ratios varying from 0.2 to 0.9 (*Konzett* and *Fei*, 2000). The recent study of *Konzett* and *Fei* (2000) shows that phase X may persist to pressures of about 20 GPa at 1500–1700 °C in bulk peridotitic compositions. In the 20–23 GPa range it breaks down to form K-hollandite, ringwoodite, majorite, Ca-perovskite and fluid. Phase X can therefore transport K, Na and H in subducting slabs and in the convecting mantle down to the boundary between the transition zone and the lower mantle.

In an anhydrous but potassium-doped peridotite composition investigated at pressures of 15–27 GPa and temperatures of 1400–2400 °C, *Wang* and *Takahashi*

(2000) recorded three different K-rich silicate phases. One of these phases (K-phase I, $K_{3.1}Na_{0.1}Ca_{0.1}Mg_{6.2}Fe_{1.5}Cr_{0.1}Al_{0.1}Si_{8.2}O_{26}$), encountered at a pressure of 15 GPa in coexistence with wadsleyite, pyroxene and garnet, is compositionally similar to the phase X reported in Table 3 ($K_{3.7}Mg_{7.4}Al_{0.6}Si_{8.0}O_{25}(OH)_2$). The two other phases encountered at pressures of 20 GPa (K-phase II) and 25.5 GPa (K-phase III) have considerably higher Al/Si-ratios and lower alkali contents. K-phase III ($K_{1.6}Na_{0.3}Ca_{0.2}Mg_{6.8}Fe_{1.1}Cr_{0.3}Al_{4.2}Si_{5.1}O_{26}$), however, is similar to a Al-K-rich phase of variable composition synthesized by *Gasparik* et al. (2000) at 24 GPa and 1700 °C. These studies indicate that there may be several minor K-rich phases present in upper parts of the lower mantle. Although the wadeite-structured $K_2Si^{VI}Si^{IV}{}_3O_9$-phase was not reported in the studies of *Konzett* and *Fei* (2000) and *Wang* and *Takahashi* (2000), this phase, accommodating 25% of its Si in octahedrally coordinated sites, is also a potential minor K-rich phase at very high pressures.

Conclusions

The decomposition of K-richterite and phlogopite at pressures above 4–5 GPa leads to mineral assemblages that largely match the starting composition of the alkaline hydrous minerals. Therefore, only minor amounts of alkali-rich hydrous fluids are formed. The fluid phases quench to fine-grained aggregates of flaky minerals that cannot be reliably analysed by electron microprobe.

The extensive stability field of K-richterite relative to phlogopite supports independent findings that phlogopite reacts with pyroxene components (diopside, jadeite and enstatite) to form potassic richterite and garnet (equation 1) in alkali-rich hydrous mantle compositions. The reaction transfers Al from 4- to 6-coordination and some of the divalent cations from 6- to 8-coordination. For a range of geothermal gradients appropriate to various subduction zone regimes, this reaction occurs gradually over the pressure interval of about 8 to 11 GPa. No hydrous fluid is released by this reaction and K-richterite appears to be stable to the upper part of the transition zone. Here K-richterite may decompose without the production of a fluid phase, because of the extensive H-solubility in wadsleyite and the occurrence of phase X and/or a wadeite-structured $K_2Si^{VI}Si^{IV}{}_3O_9$-phase as stable breakdown products.

Acknowledgements

I am pleased to be able to contribute to this remembrance of my Ph.D. advisor, *Alan Edgar*. *E. Takahashi* suggested the investigation of the stability range of K-richterite and phlogopite and provided advice and training in multianvil experimentation. Discussions with *M. Kanzaki*, *R. W. Luth* and *E. Essene*, and suggestions and corrections from *A. K. Gupta* and one anonymous reviewer were helpful. *D. Caird*, *P. Wagner*, *C. Payette* and *T. Boassen* provided technical assistance. The experimental work was supported by grants from the Natural Sciences and Engineering Research Council of Canada (major installation and infrastructure grants to *C. M. Scarfe* and an operating grant to the author), and the Geological Survey of Norway supported some of the analytical work.

References

Akaogi M, *Ito E*, *Navrotsky A* (1989) Olivine–modified spinel–spinel transitions in the system Mg_2SiO_4–Fe_2SiO_4: calorimetric measurements, thermochemical calculations, and geophysical applications. J Geophys Res 94: 15671–15685

Dawson JB (1987) The MARID suite of xenoliths in kimberlite: relationship to veined and metasomatised peridotite xenoliths. In: *Nixon PH* (ed) Mantle xenoliths. John Wiley & Sons, Chichester, pp 465–474

Erlank AJ, *Waters FG*, *Hawkesworth CJ*, *Haggerty SE*, *Allsopp HL*, *Rickard RS*, *Menzies M* (1987) Evidence for mantle metasomatism in peridotite nodules from the Kimberley pipes, South Africa. In: *Menzies MA*, *Hawkesworth CJ* (eds) Mantle metasomatism. Academic Press, London, pp 221–311

Fasshauer DF, *Wunder B*, *Chatterjee ND*, *Höhne WH* (1998) Heat capacity of wadeite-type $K_2SiSi_3O_9$ and the pressure-induced stable decomposition of K-feldspar. Contrib Mineral Petrol 131: 210–218

Fei Y, *Bertka CM* (1999) Phase transitions in the Earth's mantle and mantle mineralogy. In: *Fei Y*, *Bertka CM*, *Mysen BO* (eds) Mantle petrology: field observations and high pressure experimentation: a tribute to Francis R (Joe) Boyd. Geochem Soc Spec Publ 6: 189–207

Fei Y, *Mao H-K*, *Mysen B* (1991) Experimental determination of element partitioning and calculation of phase relations in the MgO–FeO–SiO_2 system at high pressure and high temperature. J Geophys Res 96: 2157–2169

Foley S (1991) High-pressure stability of the fluor- and hydroxy-endmembers of pargasite and K-richterite. Geochim Cosmochim Acta 55: 2689–2694

Gasparik T (1990) A thermodynamic model for the enstatite-diopside join. Am Mineral 75: 1080–1091

Gasparik T, *Tripathi A*, *Parise JB* (2000) Structure of a new Al-rich phase $(K, Na)_{0.9}(Mg, Fe)_{0.9}(Mg, Si)_2Si_6O_{20}(OH)_4$, synthesized at 24 GPa. Am Mineral 85: 613–618

Gilbert MC, *Briggs DF* (1974) Comparison of the stabilities of OH- and F-potassic richterites – a preliminary report. Eos Trans Am Geophys Union 55: 480–481

Harlow GE (1997) K in clinopyroxene at high pressure and temperature: an experimental study. Am Mineral 82: 259–269

Harte B (1987) Metasomatic events recorded in mantle xenoliths: an overview. In: *Nixon PH* (ed) Mantle xenoliths. John Wiley & Sons, Chichester, pp 625–640

Herzberg CT, *Gasparik T*, *Sawamoto H* (1990) Origin of mantle peridotite: constraints from experiments to 16.5 GPa. J Geophys Res 95 (B10): 15779–15803

Huebner SJ, *Papike JJ* (1970) Synthesis and crystal chemistry of sodium-potassium richterite, $(Na, K)NaCaMg_5Si_8O_{22}(OH, F)_2$: a model for amphiboles. Am Mineral 55: 1973–1992

Inoue T, *Yurimoto H*, *Kudoh Y* (1995) Hydrous modified spinel, $Mg_{1.75}SiH_{0.5}O_4$: a new water reservoir in the mantle transition region. Geophys Res Lett 22: 117–120

Inoue T, *Irifune T*, *Yurimoto H*, *Miyagi I* (1998) Decomposition of K-amphibole at high pressures and implications for subduction zone volcanism. Phys Earth Planet Int 107: 221–231

Katsura T, *Ito E* (1989) The system Mg_2SiO_4–Fe_2SiO_4 at high pressures and temperatures: precise determinatioons of the stabilities of olivine, modified spinel and spinel. J Geophys Res 94: 15663–15670

Kinomura N, *Kume S*, *Koizumi*, *M* (1989) Synthesis of $K_2SiSi_3O_9$ with silicon in 4- and 6-coordination. Mineral Mag 40: 401–404

Konzett J, *Fei Y* (2000) Transport and storage of potassium in the Earth's upper mantle and transition zone: an experimental study to 23 GPa in simplified and natural bulk compositions. J Petrol 41: 583–603

Konzett J, *Ulmer P* (1999) The stability of hydrous potassic phases lherzolitic mantle – an experimental study to 9.5 GPa in simplified and natural bulk compositions. J Petrol 40: 629–652

Konzett J, *Yang H* (1998) Structure and composition of phase X, a hydrous alkali-rich high pressure silicate. Eos Trans Am Geophys Union 79: F996

Konzett J, *Sweeney RJ*, *Thompson AB*, *Ulmer P* (1997) Potassium amphibole stability in the upper mantle. An experimental study in a peralkaline KNCMASH system to 8.5 GPa. J Petrol 38: 537–568

Kushiro I, *Erlank AJ* (1970) Stability of potassic richterite. Carnegie Inst Wash Yearb 68: 231–233

Kushiro I, *Syono Y*, *Akimoto S* (1967) Stability of phlogopite at high pressures and possible presence of phlogopite in the Earth's upper mantle. Earth Planet Sci Lett 3: 197–203

Luth RW (1997) Experimental study of the system phlogopite-diopside from 3.5 to 17 GPa. Am Mineral 82: 1198–1209

Luth RW, *Trønnes RG*, *Canil D* (1993) Volatile-bearing phases in the Earth's mantle. In: *Luth RW* (ed) Experiments at high pressure and application s to the Earth's mantle. Mineral Assoc Canada Short Course Handbook 21: 445–485

McKenzie D, *Bickle MJ* (1988) The volume and composition of melt generated by the extension of the litosphere. J Petrol 29: 625–679

Pawley AR (1994) The pressure and temperature stability limits of lawsonite: implications for H_2O recycling in subduction zones. Contrib Mineral Petrol 118: 99–108

Pacalo REG, *Gasparik T* (1990) Reversals of the orthoenstatite–clinoenstatite transition at high pressures and temperatures. J Geophys Res 95: 15853–15858

Peacock SM (1991) Numerical simulation of subduction zone pressure-temperature-time paths: constraints on fluid production and arc magmatism. Phil Trans Roy Soc Lond Ser A 335: 341–353

Sato K, *Katsura T*, *Ito E* (1997) Phase relations of natural phlogopite with and without enstatite up to 8 GPa: implication for mantle metasomatism. Earth Planet Sci Lett 146: 511–526

Shinmei T, *Tomioka N*, *Fujino K*, *Kuroda K*, *Irifune T* (1999) In situ X-ray diffraction study of enstatite up to 12 GPa and 1473 K and equations of state. Am Mineral 84: 1588–1594

Smyth JR, *Kawamoto T* (1997) Wadsleyite II: a new high pressure hydrous phase in the peridotite–H_2O system. Earth Planet Sci Lett 146: E9–E16

Sudo A, *Tatsumi Y* (1990) Phlogopite and K-amphibole in the upper mantle: implication for magma genesis in subduction zones. Geophys Res Lett 17: 29–32

Trønnes RG (1990) Low-Al, high-K amphiboles in subducted lithosphere from 200 to 400 km depth: experimental evidence. Eos Trans Am Geophys Union 71: 1587

Trønnes RG (2000) Melting relations and major element partitioning in an oxidized bulk Earth model composition at 15–26 GPa. Lithos 53: 233–245

Trønnes RG, *Takahashi E*, *Scarfe CM* (1988) Stability of K-richterite and phlogopite to 14 GPa. Eos Trans Am Geophys Union 69: 1510–1511

Wang W, *Takahashi E* (2000) Subsolidus and melting experiments of K-doped peridotite KLB-1 to 27 GPa: its geophysical and geochemical implications. J Geophys Res 105: 2855–2868

Wei K, *Trønnes RG*, *Scarfe CM* (1990) Phase relations of aluminum-undepleted and aluminum-depleted komatiites at pressures of 4–12 GPa. J Geophys Res 95: 15817–15827

Yagi T, *Akaogi M*, *Arashi M*, *Okai T*, *Kawamura K*, *Shino K*, *Shimomura M*, *Suzuki T*, *Tabata K*, *Akimoto S* (1987) Precise determination of the olivine–spinel phase transition in Fe_2SiO_4. J Geophys Res 92: 6207–6213

Yoder HS, *Kushiro I* (1969) Melting of a hydrous phase: phlogopite. Am J Sci 267A: 558–582

Zhang J, *Li B*, *Utsumi W*, *Liebermann RC* (1996) In situ X-ray observations of the coesite-stishovite transition: reversed phase boundary and kinetics. Phys Chem Minerals 23: 1–10

Author's address: *R. G. Trønnes*, Nordic Volcanological Institute, University of Iceland, Grensasvegur 50, IS-108 Reykjavik, Iceland, e-mail: rgt@norvol.hi.is